Geoenvironmental Disasters

RESEARCH

Open Access

Analysis of spatial distribution of landslides triggered by the Ms 6.8 Luding earthquake in China on September 5, 2022

Zikang Xiao[1,2], Chong Xu[1,2*], Yuandong Huang[1,2,3], Xiangli He[1,2], Xiaoyi Shao[1,2], Zhaoning Chen[1,2,4], Chenchen Xie[1,5], Tao Li[1,2] and Xiwei Xu[1,2,3]

Abstract

Background On September 5, 2022, an Ms 6.8 earthquake occurred in Luding County, Ganzi Tibetan Autonomous Prefecture, Sichuan, China. The casualties and economic losses caused by the earthquake are huge. Most of the landslides triggered by this earthquake are small and medium-sized rock collapses and destructive debris flows, with a small number of large-scale landslides.

Results There are 5007 coseismic landslides in the Luding earthquake VII-degree area and above, with a total area of 17.36 km^2. The landslides are generally distributed along the NW-SE direction. The highest landslide area density is 13.8%, and the highest point density of the landslide is 35.73 km^2. High-density area is mainly concentrated in the IX-degree area and the northeast side of the seismogenic fault. Coseismic landslides are more likely to develop in the area with the slope more than 40°, the slope direction of 67.5-112.5 degree, and vegetation coverage of 40–50%. More landslides are developed in granite areas and forest areas. The closer distance to active faults, the more the coseismic landslides develop. The correlation between coseismic landslide development and the distance from the active faults is better than that between coseismic landslide development and the distance from the seismogenic faults.

Conclusion The landslide database used in this paper is the most perfect at present, and the research results have also been verified by fieldwork. This is also the first applied study of this landslide inventory, which indirectly confirmed the accuracy of the inventory. The results obtained in the manuscript will provide an important guideline for futuredisaster prevention and mitigation in southwest China.

Keywords 2022 Luding earthquake, Coseismic landslides, Landslides inventory, Spatial distribution, Seismogenic structures

Introduction

Landslides and collapses are usually caused by strong earthquakes in mountain and valley areas. In addition, these areas are prone to form disaster chains to generate geological disasters, thus causing huge economic losses and serious casualties. For example, nearly 200,000 landslides were induced by the Wenchuan earthquake in 2008, with a total area of 1160 km^2 (Xu et al. 2013a). The coseismic landslides caused more than 20,000 deaths, about a quarter of the total deaths (Yin 2009). In 2013, the Lushan Ms7.0 earthquake triggered more than 1000

*Correspondence:
Chong Xu
xc11111111@126.com
[1] Ministry of Emergency Management of China, National Institute of Natural Hazards, Beijing 100085, China
[2] Key Laboratory of Compound and Chained Natural Hazards Dynamics, Ministry of Emergency Management of China, Beijing 100085, China
[3] China University of Geosciences (Beijing), Beijing 100083, China
[4] School of Emergency Management Science and Engineering, University of Chinese Academy of Sciences, Beijing 100049, China
[5] Institute of Disaster Prevention, Sanhe 065201, China

landslides, resulting in the complete blockage of many roads in the mountain area, and seriously affecting the transportation of residents (Chen et al. 2013). The 2014 Ludian Ms6.5 earthquake not only induced large landslides such as Ganjiazhai, Wangjiapo, and Hongshiyan but also caused a sharp increase in potential geological hazards. According to statistics, the number of potential geological hazard points after the earthquake was 4.4 times than before, which posed a continuous threat to local socio-economic development and human safety (Yang and Yao 2018).

The study of seismic landslide distribution characteristics should be based on a large number of landslide data (Harp et al. 2011). New and emerging techniques based on satellite, airborne, and terrestrial remote sensing technologies, promote research on the distribution characteristics of coseismic landslides (Guzzetti et al. 2012). At the present stage, the analysis of the distribution characteristics of coseismic landslides is no longer limited to the statistics of the number, type, mode, and other parameters. For example, Based on the list of earthquake landslides, Cui et al. (2022) not only analyzed the distribution characteristics of coseismic landslides in the Tonghai earthquake but also compared the landslide parameters in different earthquake events, making people a clearer understanding of the disaster degree of the Tonghai earthquake. He et al (2021) established an inventory of Qiaojia earthquake landslides, focusing on the relationship between LND and LAP and active faults, and deduced the seismogenic fault of the earthquake. Chang et al. (2021) analyzed the correlation between the spatial distribution characteristics of landslides induced by the 2013 Lushan earthquake and the 2017 Jiuzhaigou earthquake and the seismic, topographic, geological and other control factors. They also summarized the distribution characteristics of coseismic landslides in southwest China and provided a scientific basis for emergency rescue work. Thus, establishing earthquake-induced geological disasters inventory immediately after the earthquake, and analyzing the spatial distribution pattern, formation mechanism, and main control factors of coseismic landslides play an important role in guiding the prevention and prediction of geological disasters after the earthquake (Keefer 2000; Dai et al. 2011; Shao et al. 2022).

On September 5, 2022 (Beijing time), in Luding County (102.08° E, 29.59° N), Ganzi Tibetan Autonomous Prefecture, Sichuan Province, China, an Ms6.8 strong earthquake occurred with a focal depth of 16 km (China Earthquake Networks Center, www.ceic.ac.cn). According to the seismic intensity map released by the China Earthquake Administration of the Ministry of Emergency Management, the highest seismic intensity caused by the earthquake reached IX degree, with an area of 280 km^2. The long axis of the isoseismal line is northwest. The area of the VI-degree and above is 19089 km^2, involving 3 cities (prefectures), 12 counties (cities, districts), and 82 towns (streets) in Sichuan Province. As of September 13, this earthquake caused a great loss of people and property, including 93 deaths and 25 missing, triggered a large number of geological disasters such as collapses and landslides, and destroyed a large number of houses and roads (Fan et al. 2022; Li et al. 2022; Wang et al. 2022). After the earthquake, Huang et al. (2022) quickly established an inventory of Luding earthquake coseismic landslides. In this paper, based on the landslide database established by Huang et al. (2022), and taking the Luding earthquake VII degree area and above as the study area, we analyzed the spatial characteristics and influencing factors of coseismic landslides from the seismic, topographic, and geological perspectives, and discussed the relationship between the seismogenic structure and the coseismic landslides.

Geologic setting and historical earthquake

The earthquake area is located in the Hengduan Mountains on the southeast of the Qinghai Tibet Plateau, which is a typical mountain canyon landform. Dadu River runs through the area from north to south, with a large drop. The epicenter was in Hailuogou Glacier Forest Park, Gongga Mountain. Gongga Mountain is 7556 m above sea level, with an elevation difference of 6570 m. The lithology formation in this area is mainly granite in Early Sinian, monzonite in Tertiary, dolomite in Permian Leikoupo Formation, etc. Due to long-term strong tectonic and weathering, the rock and soil mass is broken, which provides favorable conditions for the occurrence of geological disasters (Li et al. 2022).

The Luding earthquake occurred near the Moxi fault in the southeast segment of the Xianshuihe fault zone on the southeast margin of the Qinghai Tibet Plateau. Xianshuihe fault zone is one of the boundary strike-slip fault zones with strong activity and large scale, which regulate the relative motion and extrusion of various sub-plates under the background that the convergence of Indian and Eurasian plates continuously extrudes the crustal materials on the southeast edge of the Qinghai Tibet Plateau to the southeast (Tapponnier and Molnar 1977; Wang and Burchfiel 2000; Tapponnier et al. 2001) (Fig. 1a). It is located at the boundary between the Bayan Har block and the Sichuan-Yunnan block on the eastern margin of the Qinghai Tibet Plateau and intersects with the Longmen Mountain fault zone and the Anning River fault zone to form the famous 'Y-shaped' fault zone in western Sichuan (Wang and Li 2015) (Fig. 1b). The Xianshuihe fault zone is 350 km long, starting from the northwest area of Donggu in the north and extending to the south

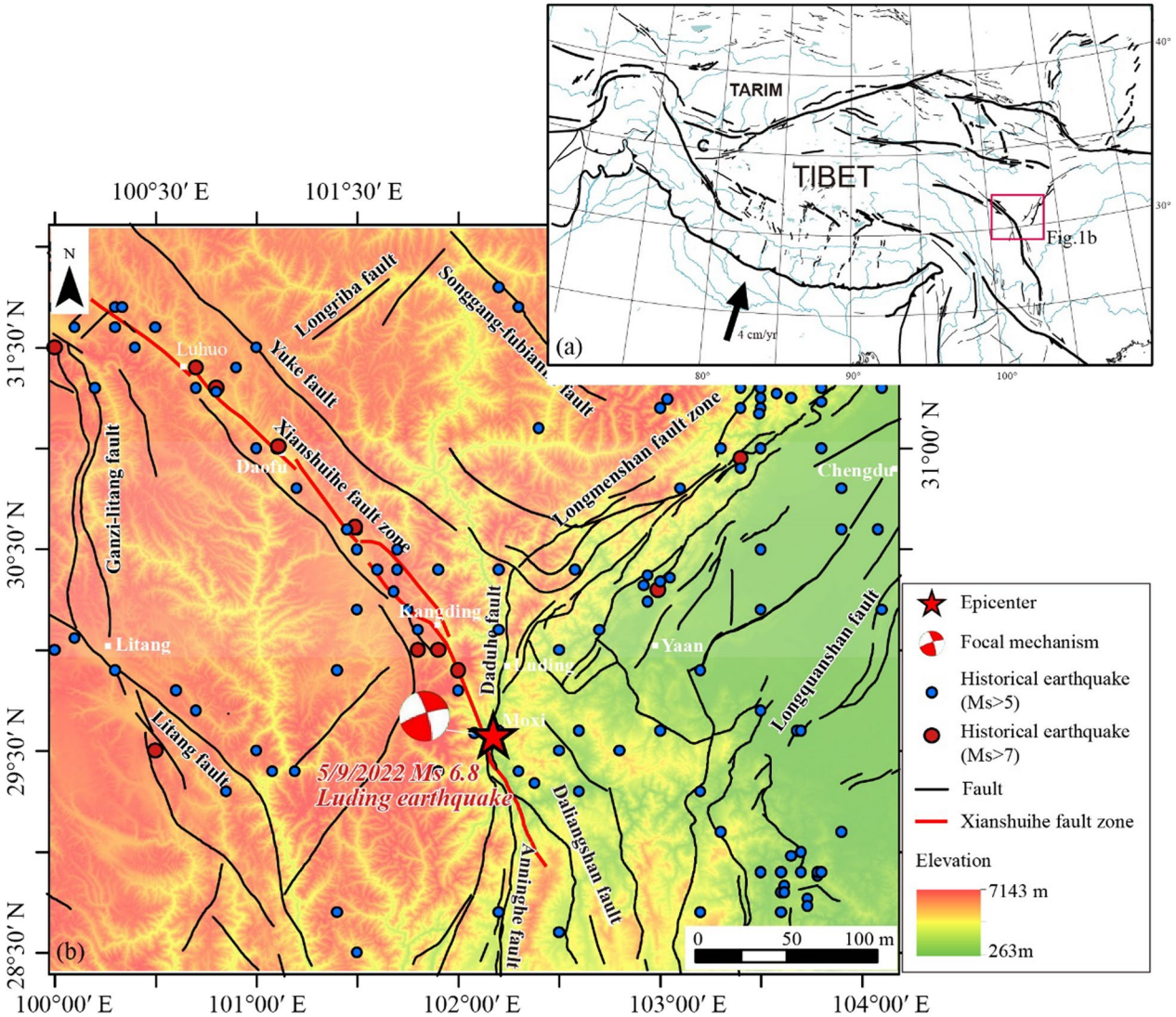

Fig. 1 Regional tectonic background and historical earthquake distribution map of Ms6.8 Luding earthquake on September 5, 2022. **a** Structural background of the Qinghai Tibet Plateau and its adjacent areas. **b** Tectonic background and historical earthquake distribution map of the seismic area

of Moxi. The NW section can be divided into the Luhuo section, the Daofu section, and the Qianning section from NW to SE, with a strike of about N130°–148°. The NW section tends to NE, and the SW trending fault can be seen locally (Tang and Qiang 1984; Bai et al. 2021). The SE section, from Huiyuansi to Kangding, is composed of four branch faults: Yalahe fault, Selaha fault, Mugecuo south fault, and Zheduotang fault, with a strike of about 145° (Pan and Li 2020). Subsequently, the Xianshuihe fault continued to extend southward, connecting with the Moxi fault with a strike of about 160° near Kangding and finally reaching Moxi Zhenfu. The northwestward Xianshuihe fault zone, Ganzi fault, Yushu fault, Batang fault, Dangjiang fault, and the southward Anning River fault, Zemuhe fault, and Xiaojiang fault constitute a huge sinistral strike-slip fault system (Xianshuihe fault system), forming the eastern boundary of Sichuan-Yunnan diamond block with a span of 1400 km (Wen and allen. 1989; Allen et al. 1991; Kato et al. 2007). In terms of the characteristics of fault movement, Zheng et al. (2017) believed that the Xianshuihe fault, to adapt to the clockwise rotation of the Qinghai Tibet Plateau relative to the South China plate in the Himalayan tectonic movement, showed a left-handed displacement of 9 mm/yr and a normal fault slip of 1–3 mm/yr. Bai et al. (2022) concluded that the average strike-slip rate of the Xianshuihe

fault system in the late Quaternary gradually increased from the NW Ganzi fault to the SE.

Xianshuihe fault zone is one of the most active fault zones in mainland China and an important part of the north–south seismic zone (Deng et al. 2003; Wen et al. 2008; Zhang 2013). Destructive earthquakes occur frequently in this fault zone (Fig. 1b). Since 1700, 17 earthquakes with magnitude above 7 have occurred along the Xianshuihe fault system, and 9 of them were located in the Xianshuihe fault zone in the middle of the fault system (Fig. 1b) (Bai et al. 2022). The closest one to the Luding earthquake was the Luding Ms7.75 earthquake on June 1, 1786. The most recent one was the Luhuo Ms7.9 earthquake in Sichuan on February 6, 1973. In addition, the Ms8.0 Wenchuan earthquake in 2008 and the Ms7.0 Lushan earthquake in 2013 occurred in the Longmenshan fault zone, which are within 300 km of this area. Relevant researches show that after the two earthquakes, the Coulomb failure stress changes (ΔCFS) near the Xianshuihe fault has increased obviously, and the seismic risk has also increased significantly (Toda et al. 2008; Shan et al. 2009; Xu et al. 2013b; Wu et al. 2014; Xiong et al. 2016; Guo et al. 2018).

Data and methods

Landslides interpretation based on remote sensing image. Accurate and detailed landslide data cataloging is the basis of landslide research (Shao and Xu 2022; Zhang et al. 2022; Huang et al. 2022b). Since the earthquake occurred recently, the difference between the hue and shape of the landslide image and the surrounding ground objects is obvious. Therefore, we adopt the combination of visual interpretation based on optical satellite images and field investigation to establish the landslide catalog. The source of the optical satellite image is Planet satellite data, and the imaging time is July and September 29, 2022, respectively. Through the comparison of image

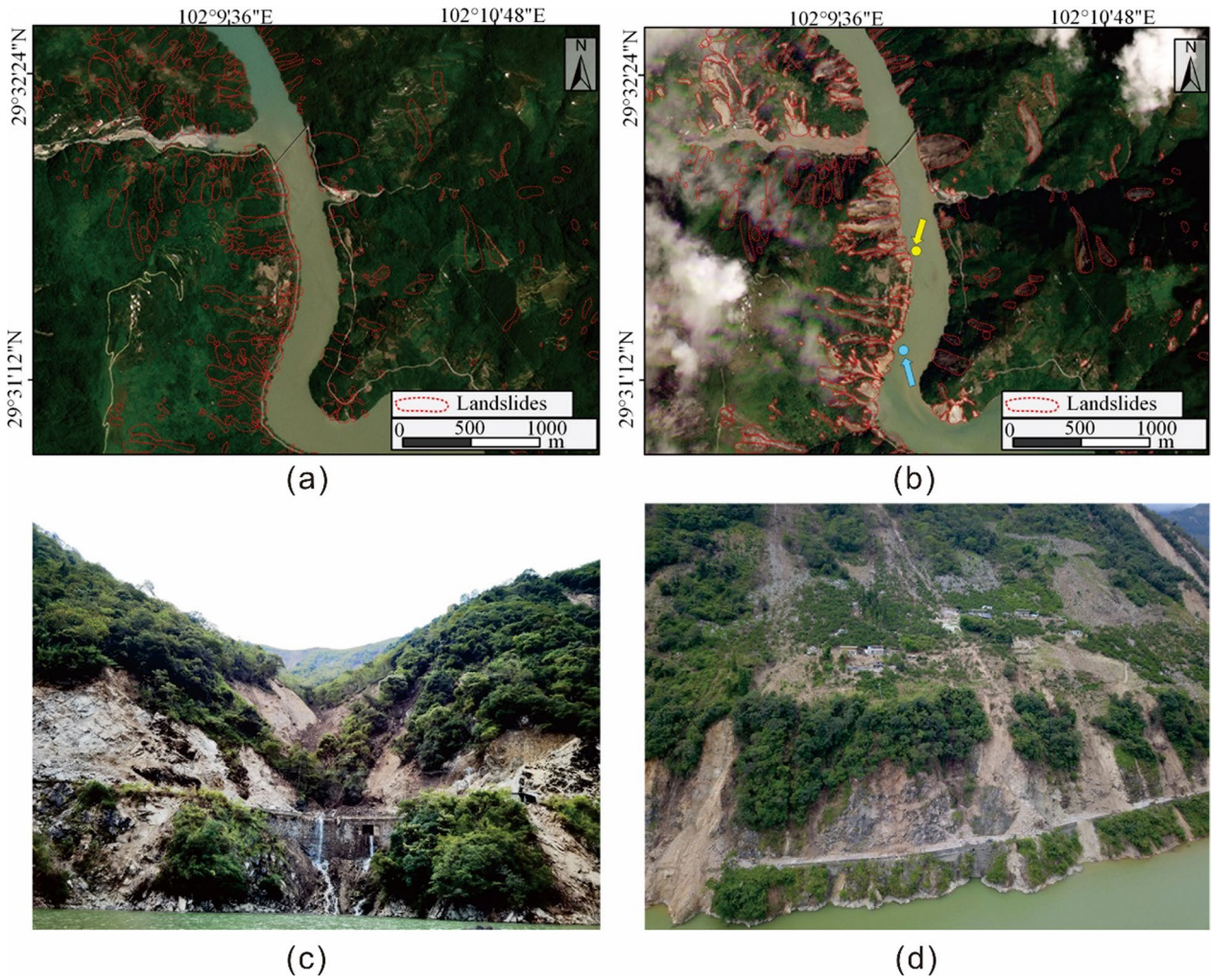

Fig. 2 Remote sensing image of landslide area before and after earthquake and field photos. **a** And **b** are the pre and post-earthquake images of the same area (Planet Team 2022). **c** And **d** are field photos of the yellow and blue mark positions in (**b**), respectively

features before and after the earthquake, the interpretation result of this coseismic landslide becomes more accurate. Figure 2 shows a high-density development area of coseismic landslides (Fig. 2).

Influencing factors of coseismic landslides

The main factors controlling the development characteristics of coseismic landslides are seismic, geologic, and topographic. In this paper, the seismic intensity, and the distance to the seismogenic fault are selected as seismic factors. Elevation, slope, and aspect are selected as topographic factors. Stratigraphic lithology, land use type, vegetation coverage, and distance from active fault are selected as geologic factors. Finally, a total of 9 characteristic parameters are used as the influencing factors of the coseismic landslide to carry out the research.

The study area in this paper is the VII-degree area, VIII-degree area, and IX-degree area of the Luding earthquake, with a total area of 4393 km^2. Taking ALOS PALSAR DEM (resolution: 25 m) as the basic data, the slope data is obtained by using GIS spatial analysis technology. The lithological data is obtained based on the 1:200000 national geological map (Li et al. 2019). Generate vegetation coverage data are obtained based on the latest results of global land use types. By using the buffer zone analysis method, the distance grid data from the fault structure in the study area are obtained. The data on earthquake intensity and epicenter are all from the data published by China Earthquake Networks Center.

Except for lithological data, other data are in grid form, so the grid value of the landslide location can be directly extracted for statistics. The lithological data is a vector with many field attributes. Referring to relevant research, we adopt the stratigraphic age as the classification standard for sedimentary rocks and metamorphic rocks and divide magmatic rocks according to their material composition (acidic ultrabasic), including granite, diorite, etc.

Table 1 Descriptions of categorized lithology in the study area

Lithology number	Period	Petrographic description
1	Q	Loose gravel layer, sand, and clay
2	N	Basic rock
3	T	Sandstone, siltstone, shale, and dolomite
4	P	Basalt, tuff, breccia, marble and alate
5	D	Sandstone, siltstone, shale, and limestone
6	S, O, Z	Others, include Ordovician, Silurian, Sinian, etc
7	Σ	Ultrabasic rock
8	γ	Granite, biotite granite, granitic migmatite, and monzogranite
9	δ	Diorite, quartz diorite, and granodiorite

The specific lithological classification and description are shown in Table 1.

In terms of evaluation indicators for the development of coseismic landslides, the number and area of landslides are commonly used as statistical indicators (Zhao et al. 2021), and both of them can directly reflect the distribution of landslide disasters. In addition, considering that there may be large differences in the scale and area of some factor intervals, the percentage of landslide area (LAP) was added as the evaluation index. It is defined as the ratio of the landslide area within the section to the total area of the section, which can reflect the relative advantages of landslide development.

According to the above analysis, based on the GIS platform, a variety of technologies and tools including spatial surface analysis, grid calculation, and distance division were adopted to finally obtain the distribution map of coseismic landslides influence factors in the Luding Seismic Intensity XII-degree and above areas (Fig. 3).

Results

Landslides distribution

In combination with the visual interpretation of remote sensing images and field surveys, we established a detailed landslide inventory of the Luding earthquake in 2022 (Huang et al. 2022a). According to statistics, there are 5007 coseismic landslides in the VII-degree area (Fig. 4), with a total area of 17.36 km^2. The maximum landslide area is 120747 m^2, the minimum landslide area is 65 m^2, and the average landslide area is 3466.78 m^2. There are 327 landslides with an area of more than 10,000 m^2 and 3099 landslides with an area of 1000–10,000 m^2 totally. The landslides are generally distributed along the NW–SE direction. Most landslides are medium and small rock collapses and destructive debris flows, with a small number of large-scale landslides.

To further study the distribution trend of the landslides, we use the Gaussian kernel density estimator to calculate the area density and point density of landslides in the study area.

Gaussian kernel density calculator is a common tool for calculating area density and point density in GIS software. Its core idea is to use the kernel function to calculate the unit area size of point features, so as to fit the smooth conical surface to each point or multiple lines. The functional formula of kernel density estimation is:

$$f_n(x) = \frac{1}{nh}\sum_{i=1}^{n} k\left(\frac{x - x_i}{h}\right)$$

where K is the weight function of the kernel, h is the bandwidth, $x - x_i$ is the distance between the density estimation point x and x_i.

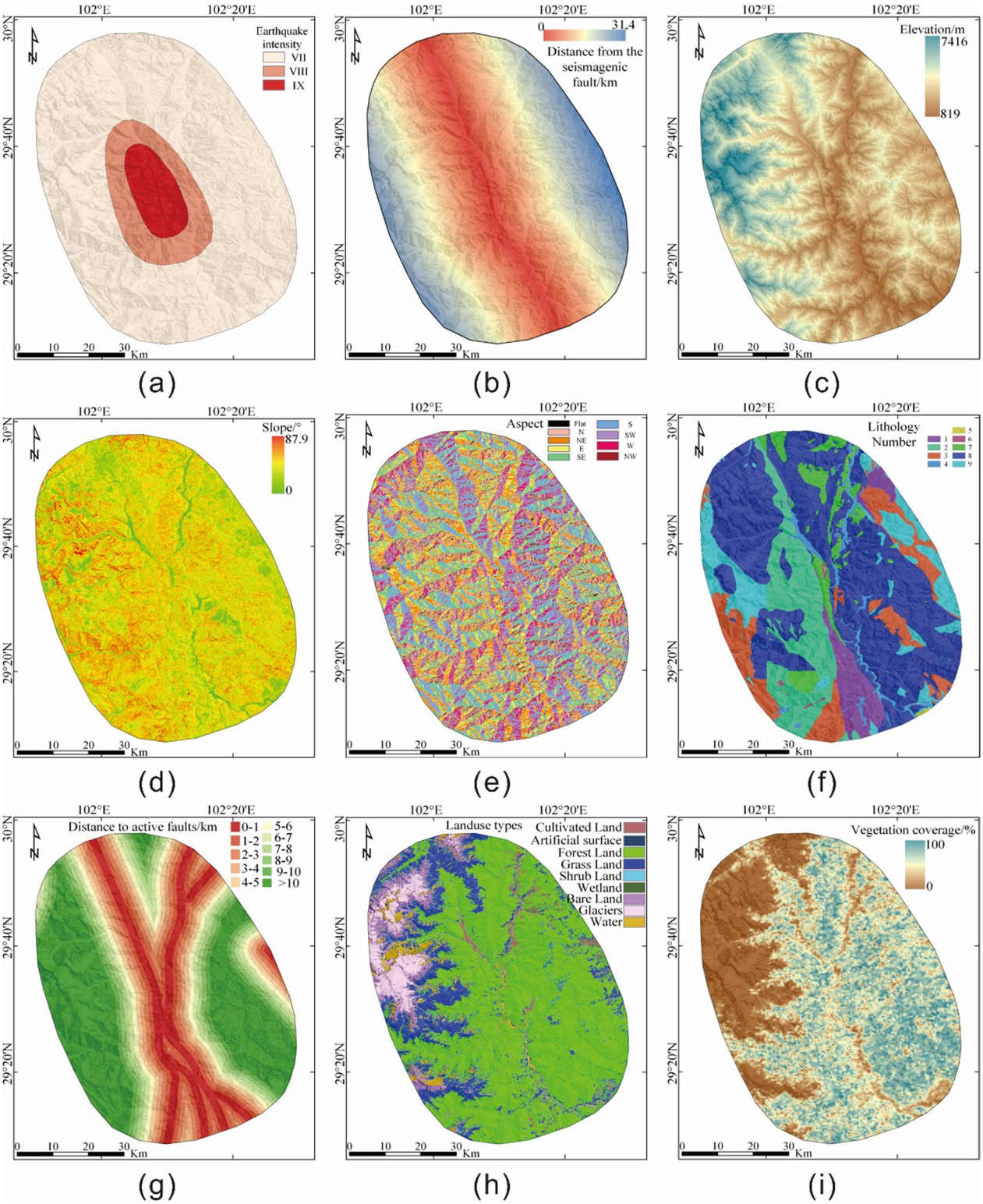

Fig. 3 Maps showing the distribution of the influencing factors in the study area. **a** Earthquake intensity. **b** Distance to seismogenic fault. **c** Altitude. **d** Slope. **e** Aspect of slope **f** Lithology. **g** Distance to active fault. **h** Land use type. **i** Vegetation coverage

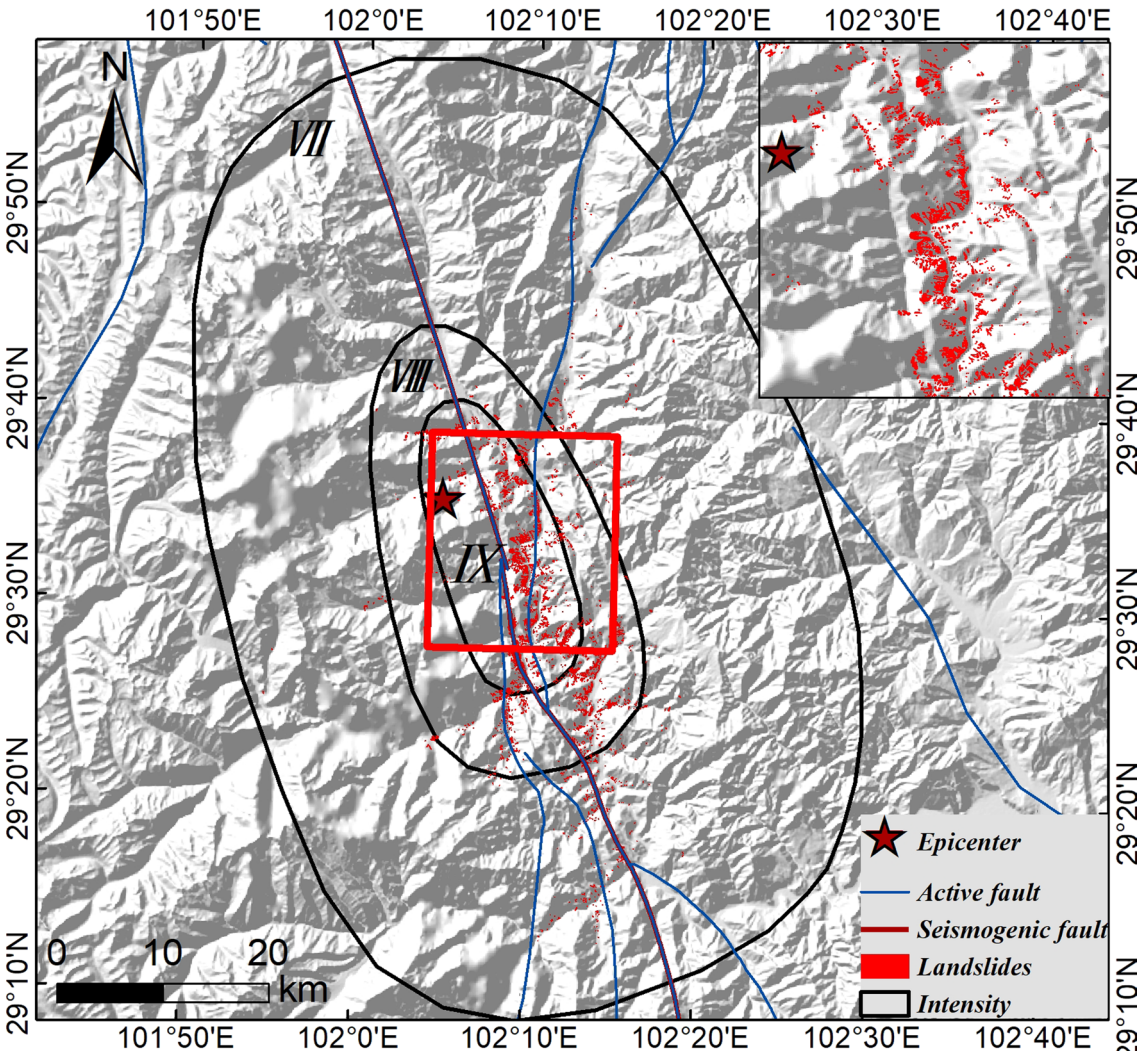

Fig. 4 Coseismic landslides distribution map, modified from Huang et al. (2022a). The black line is seismic intensity downloaded from https://www.cenc.ac.cn/

In the area with a large number of points, the nuclear density value is also high. Considering that there are many landslides in the study area, our search radius is set to 2 km, and the calculation results are shown in Fig. 4.

Considering that there are a large number of landslides in the study area, the search radius is set as 2 km, and the results are shown in Fig. 4. The highest landslide area density is 13.8%, and the highest point density of the landslide is 35.73 km^2. High density area is mainly concentrated in the IX-degree area and the northeast side of the seismogenic fault (Fig. 5).

Correlation between landslides distribution and influence factors

Seismic factors

Seismic intensity represents the severity of the impact of earthquakes on surface buildings and facilities and reflects the impact of earthquakes on the regional geological environment. Figure 6 shows the index distribution of landslide quantity, landslide area, and LAP in different intensity areas. From the inner circle to the outer circle, landslide area, LAP, and landslide quantity are respectively shown. It can be seen from the figure that in terms of landslide area and LAP, the IX-degree area interval accounts for the largest percentage, accounting for 59.7% and 78.6% respectively. In terms of the number of landslides, although the proportion of IX-degree area is less than 50%, it is still the group with

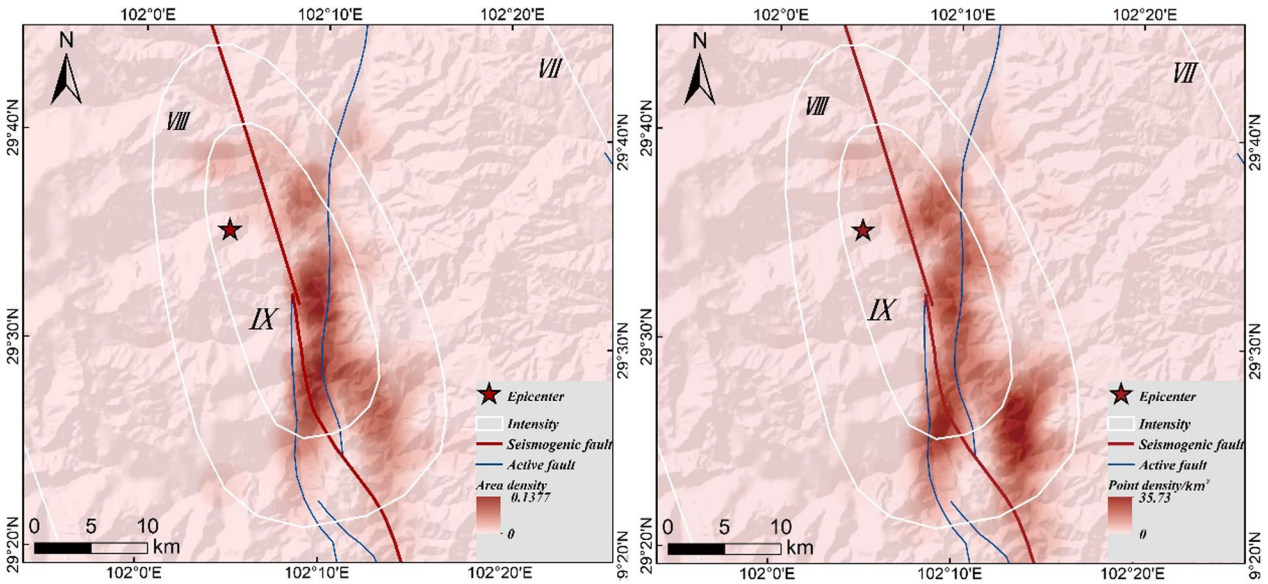

Fig. 5 Seismic Landslide Density Map. **a** Landslide area density (LAD). **b** Landslide number density (LND)

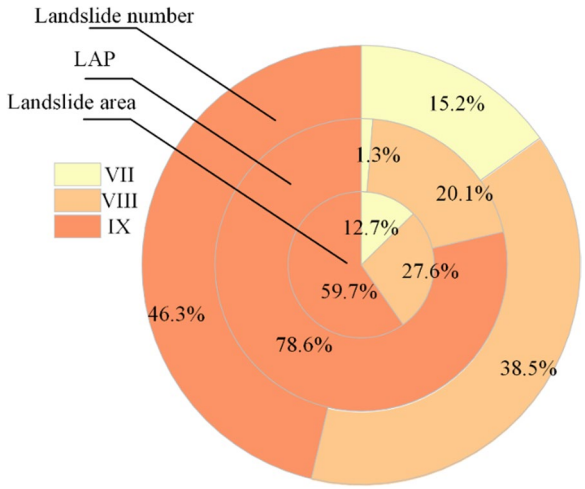

Fig. 6 Analysis diagram for landslide evaluation index and seismic intensity

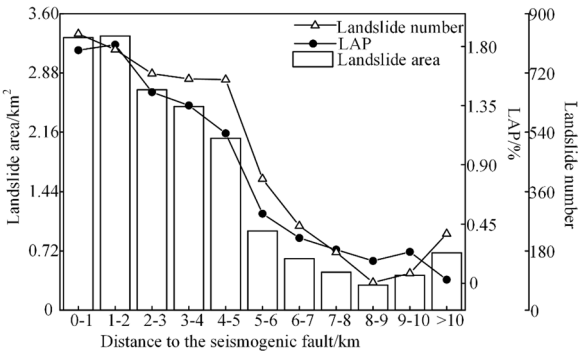

Fig. 7 Analysis diagram for landslide evaluation index and distance to seismogenic fault

the largest number of landslides, with 2321 landslides in total, and the landslide area is 10.36 km^2.

Energy of seismic waves is the direct factor causing the coseismic landslide. The seismogenic fault is the key content in the study of earthquake disasters, and an important factor in earthquake energy transmission. At present, the research on this earthquake generally believes that the Xianshuihe fault zone is the earthquake generating fault (Yang et al. 2022). Based on this, this paper studies the influence of fault distance on the development characteristics of coseismic landslides.

Generally, in the area 10 km beyond the seismogenic fault, the attenuation of seismic energy leads to a significant reduction in its impact on landslides (Wu et al. 2018). Therefore, the author merges the intervals that are more than 10 km away from the seismogenic fault and divides the intervals of other regions with an interval of 1 km. The statistical results are shown in Fig. 7. With the increasing distance to the seismogenic fault, the indicators of the landslide show a downward trend on the whole, and only show small fluctuations in some range. Among them, 839 landslides with an area of 3.31 km^2 are developed within the range of 0–1 km from the seismogenic fault, which is the maximum in each range.

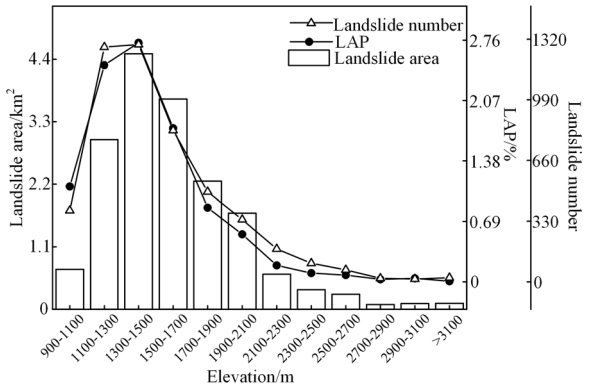

Fig. 8 Analysis diagram for landslide evaluation index and elevation

Topographic factors

Seismic factors are the reflection of landslide triggering factors and initiation mechanism, while topographic factors are the embodiment of disaster pregnant environment. In this paper, elevation, slope, and aspect are selected as the representatives of topographic factors to analyze the influence of topographic characteristics on the distribution of coseismic landslides in the study area. Figure 8 shows the index distribution of landslides in each elevation range. It can be found that the coseismic landslide has obvious development advantages in the range of elevation 1300–1500 m. There are 1291 landslides developed in the study area in this group, with a total area of 4.5 km^2 and LAP of 2.73%. All indicators are the maximum values of each group.

The slope are grouped at 10° intervals. Figure 9 shows the statistics of the evaluation indexes of the coseismic landslides of each group. It can be found that the maximum landslide area is 7.38 km^2, and the corresponding slope is 50°–60°. The maximum LAP is 2.69%, and the corresponding slope is 70°–80°. The maximum number of landslides is 2020 with a slope of 40°–50°. The comprehensive analysis shows that the area with a slope of more than 40° is favorable for landslide development.

The difference in slope direction will cause a difference in seismic energy transmission (Huang and Li 2009). The statistical results of the landslide aspect in the study area are shown in Fig. 10. It can be clearly seen that all statistical indicators of the landslide reach the maximum value in the slope direction 67.5–112.5, which corresponds to the east direction. In addition, the indicators in the northeast and southeast directions are also higher than those in other regions.

Geological factors

The geological environment is also one of the important factors affecting the development of coseismic landslides. In this paper, lithology, distance from active faults, vegetation cover, and land use type are selected as geological factors in the analysis of development characteristics of coseismic landslides. The statistical results of the four factors are shown in Fig. 11.

In terms of lithology, the number and area of landslides reach the maximum in the No. 8 lithologic group dominated by granite (Fig. 11a). 2522 landslides are developed in this group, with an area of 7.45 km^2. The LAP changes in each lithologic group are complex, which is mainly caused by the large area difference of each lithologic group. For example, in the No. 2 lithology group, LAP is 1.11%, which is relatively high. However, the number of landslides is 66, with an area of 0.182 km^2, and its group area is only 16.43 km^2. The large area difference between lithological groups leads to the large variation range of LAP, which is the most common phenomenon in the discrete factor. Therefore, it is necessary to conduct a

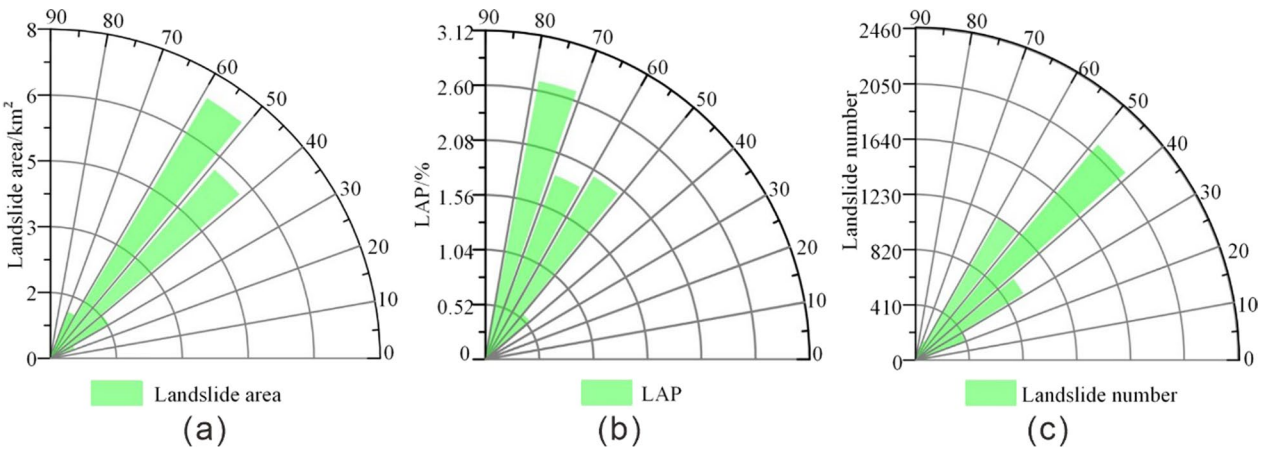

Fig. 9 Analysis diagram for landslide evaluation index and slope

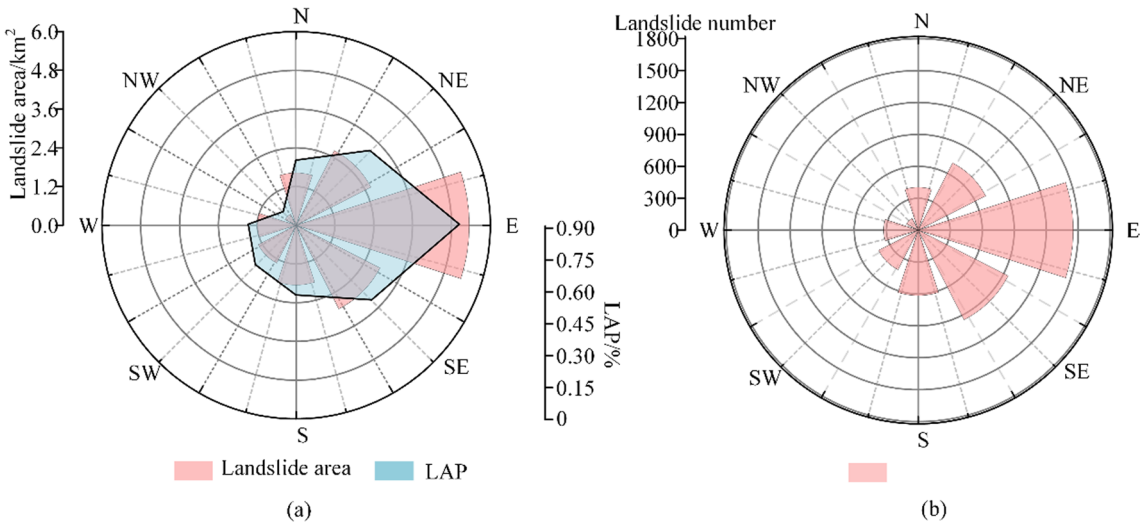

Fig. 10 Analysis diagram for landslide evaluation index and aspect of slope

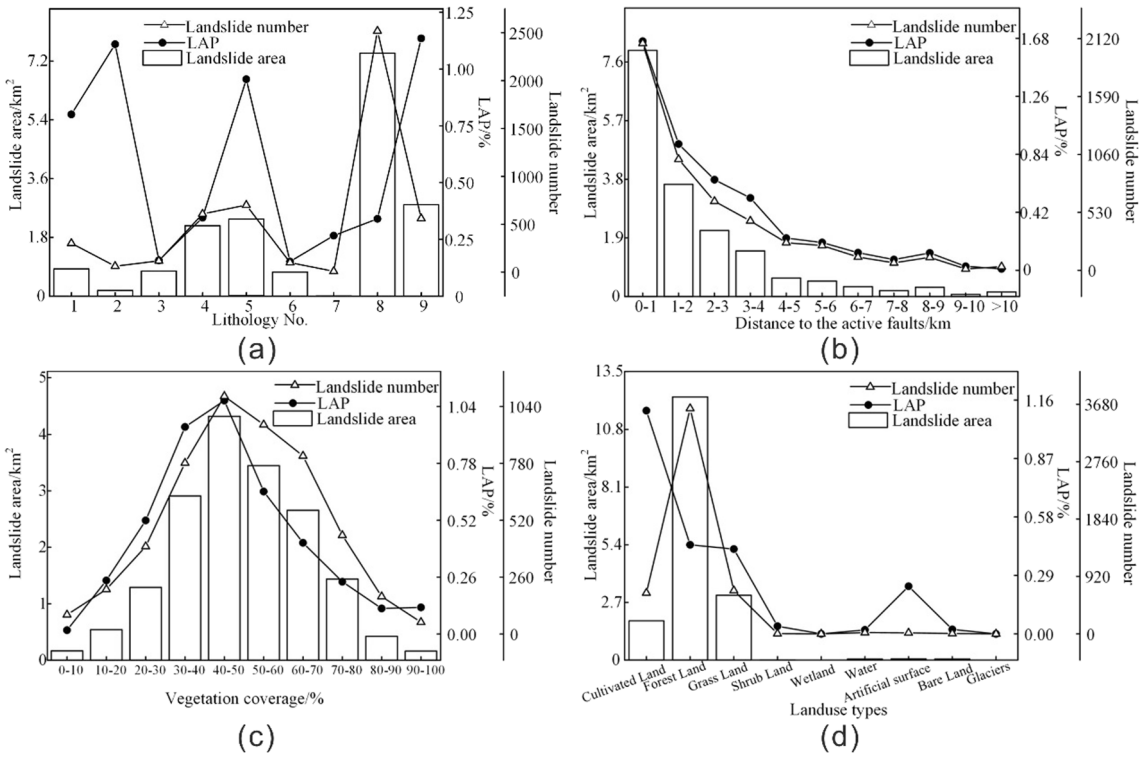

Fig. 11 Distribution of geologic factors within landslides. **a** Lithology. **b** Distance to active faults. **c** Vegetation coverage **d** Landsue type

comprehensive analysis of multiple indicators when describing the development characteristics of coseismic landslides.

Active faults are widely distributed in the study area. It can be seen from Fig. 11b that the closer to the active fault, the higher the indicators of the coseismic landslide. Compared with the distance from the seismogenic fault, it is found that the distance from the active fault has a better correlation with various indicators of landslides. Therefore, the author believes that the distribution of coseismic landslides in this earthquake is not only

affected by the seismogenic fault but also controlled by other active faults.

In terms of vegetation coverage, in the area with 40–50% vegetation coverage, the three evaluation indexes of coseismic landslides reached the maximum, respectively corresponding to 4.32 km^2 of landslide area, 1.07% of LAP1.07 and 1087 landslides (Fig. 11c).

In terms of land use type, there are obvious advantages in the development of coseismic landslides in the forest land area (Fig. 11d). The number of landslides reaches 3613, and the total area of landslides is 12.32 km^2. LAP is the largest among cultivated areas, which is 1.11%.

Discussion

Comparison of coseismic landslide inventories

After the Luding earthquake, many researchers quickly carried out investigation on the cataloging of coseismic landslides and published many papers. Wang et al. (2022) interpreted 104 km^2 of UAV aerial images and 312 km^2 of satellite images by combining model prediction with manual identification and finally obtained 3633 coseismic landslides with a total area of 13.78 km^2. Tie et al. (2022) obtained 234 landslide disaster points and 331 collapse disaster points by combining field investigation and optical satellite image interpretation.

Based on the field survey data and optical satellite image data, Huang et al. (2022) conducted coseismic landslide interpretation for the Luding earthquake VII-degree area and above. The interpretation area reaches 4393 km^2, and 5007 coseismic landslides are obtained, with a total area of 17.36 km^2. Although due to cloud cover, there are still areas that are not fully interpreted in the study area. However, compared with other scholars' research, it can be found that the landslide inventory established by Huang et al. (2022a) has larger coverage and more landslides than the others, which is the most comprehensive coseismic landslide inventory in the current study of the Luding Earthquake.

Based on the inventory established by Huang et al. (2022a), this paper has carried out the correlation analysis of coseismic landslide and seismic, geological, and topographic factors, and the results obtained are basically consistent with previous studies. There are only slight differences in slope and distance between seismogenic faults. For example, Fan et al. (2022) believed that the area with a slope of 50°–55° is more likely to develop landslides, but in this study, the maximum LAP is in the area with a slope of 70°–80°. In terms of the distance between the coseismic landslide and the seismogenic fault, Fan et al. (2022) believed that the coseismic landslide was mainly distributed within 1 km from the seismogenic fault. When the distance was more than 1 km, the landslide density decreased significantly. However, in this study, the number and density of coseismic landslides are at a high level within 0–5 km from the seismogenic fault, and there is no decreasing trend. The author speculates that the incompleteness of the study area and the misjudgment of the coseismic landslide are the main reasons. Because, in the field survey of Tie et al. (2022), there are a large number of coseismic landslides distributed in the northeast of the epicenter outside the IX-degree area, which is consistent with the landslide development characteristics obtained in this study. However, these landslides did not appear in the research scope of Fan et al. (2022) and Wang et al. (2022).

To sum up, a complete coseismic landslide database is the research basis for analyzing the spatial distribution, formation mechanism and main control factors of coseismic landslides. Based on the relatively complete Luding earthquake coseismic landslide inventory at this stage, we analyzed the main influencing factors of the coseismic landslide. Compared with the previous research results, we have some further new understanding, which are also supported by the field work. Therefore, this study could be used as a reference for the follow-up geological disaster prevention and prediction in this area.

Analysis of seismogenic structures

Earthquakes often release the energy accumulated for a long time through strong shaking or surface deformation. The energy near the epicenter and seismogenic structure are most concentrated, so coseismic landslides are often concentrated around the epicenter and seismogenic structure (Keefer 2000; Mahdavifar et al. 2006; Meunier et al. 2013; Gorum et al. 2014; Xu et al. 2014; Valagussa et al. 2019; He et al. 2021). The movement properties of seismogenic structures have certain constraints on the spatial distribution characteristics of landslides. For example, the seismogenic structures of strike-slip earthquakes tend to have a high angle occurrence of nearly 90°, and the coseismic landslides distributed on both sides of the seismogenic fault are relatively symmetrical (Gorum et al. 2014; Xu and Xu 2014). The seismogenic tectonic plane of thrust or normal fault earthquakes is inclined, and the energy is concentrated in the hanging wall of the fault. Therefore, there are many landslides developed in the hanging wall of the fault (Tatard and Grasso 2013). In addition, some earthquake fractures did not reach the surface, but only occurred in hidden faults. The earthquake energy is partially absorbed and digested, and the landslide induced by them is relatively small and distributed dispersedly (Xu and Xu 2014; He and Xu 2022). Therefore, the spatial distribution pattern of coseismic landslides can provide an important basis

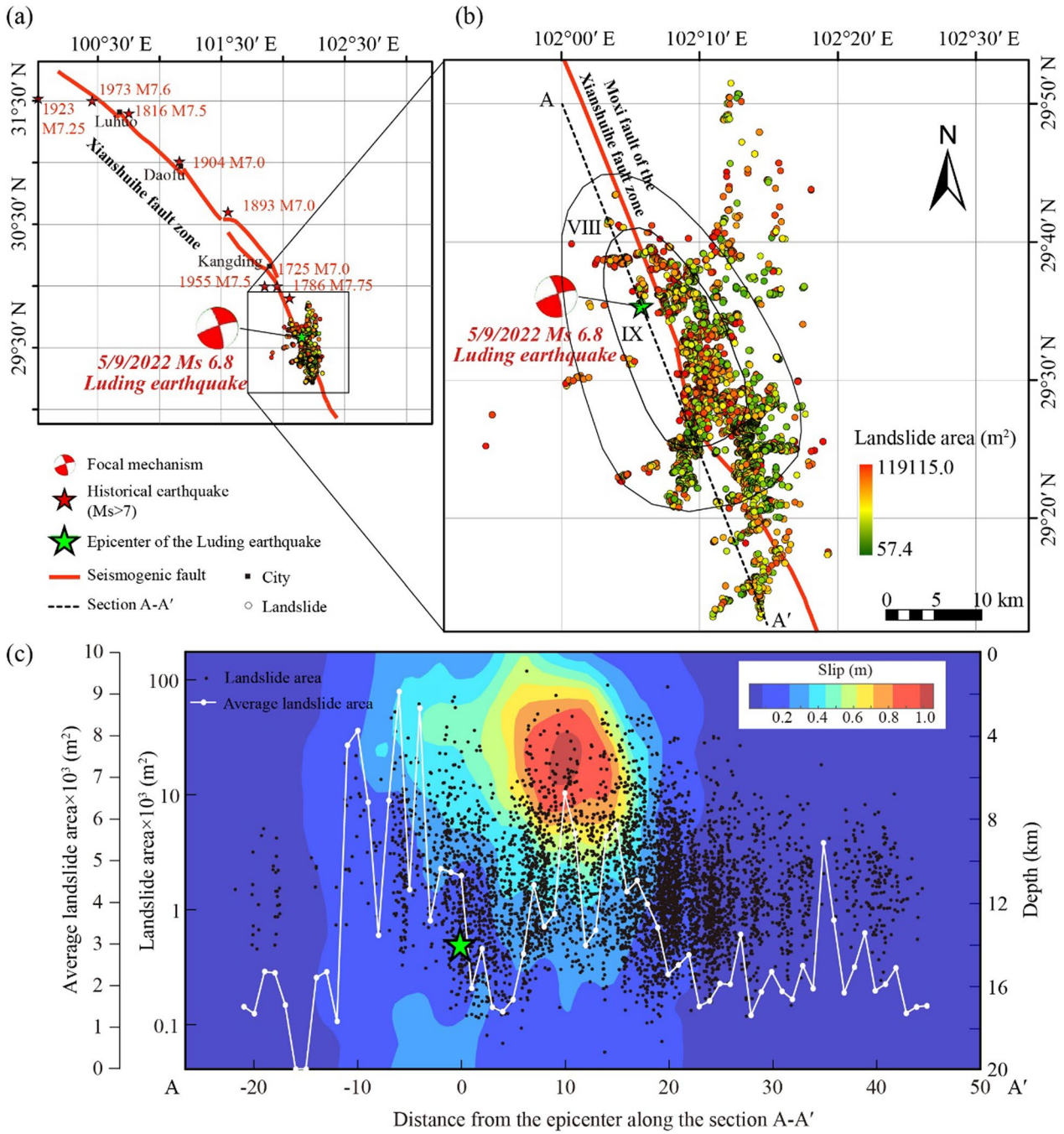

Fig. 12 The relationship between the distribution of coseismic landslides and the seismogenic fault and rupture process of Luding earthquake. **a** Historical earthquakes of Ms ≥ 7 in Xianshuihe fault zone. **b** Distribution characteristics of coseismic landslides along the Moxi fault of the Xianshuihe fault zone. **c** Coseismic landslide area along the Moxi fault strike profile. The white broken line is the average area of landslide per kilometer, the base map shows the projection of earthquake slip on the fault plane, and the green pentagram represents the location of the main earthquake source

for understanding the seismogenic structure and fracture mechanism.

The coseismic landslide of the Luding earthquake is distributed along the Moxi fault of the Xianshuihe fault zone in an NW–SE direction, consistent with the long-axis direction of the seismic intensity (Fig. 12b). The focal mechanism solution results show that the earthquake is a left-handed strike-slip earthquake with a steep dip

angle, which is consistent with the nature and geometric characteristics of Moxi fault movement. Therefore, it is inferred that the Moxi fault is the seismogenic fault of the 2022 Ms6.8 Luding earthquake. According to the distribution pattern of strike-slip fault type coseismic landslide, the landslide should be symmetrically distributed on both sides of the seismogenic fault. The landslides obtained from this interpretation are more distributed on the northeast side of the fault, which seems to indicate that the fault leans to the northeast. However, according to the field survey results and aftershock precise positioning results, the fault leans slightly to the southwest. This difference is probably because the remote sensing images on the west side of the fault are mostly obscured by clouds and cannot be interpreted, thus causing the loss of some coseismic landslides on the west side of the fault.

In addition, we projected the interpreted landslides and their areas onto the profile along the strike of the fault and found that more than 90% of the landslides were distributed in the southeast region of the epicenter, but the average area of the landslides in the northwest was larger, and the average area of the landslides in the southeast decreased as the distance from the epicenter increased (Fig. 12c, white broken line). This phenomenon illustrates that the earthquake rupture mainly propagates to the southeast section, but the rupture is shallow in the northwest and deep in the southeast. This result is consistent with the rupture process of the main shock obtained by Yang et al. (2022) using IDS method based on the waveform data of strong earthquake stations within 60 km around the main shock. They believed that the duration of the main earthquake was 18 s, which was mainly manifested by the unilateral rupture of the SSE direction, with a transverse length of 25 km and a longitudinal length of 15 km. It can also be seen from Fig. 2c that there is an obvious peak in the area 0–10 km northwest of the epicenter, and the landslide area near the epicenter is relatively small. Along the strike, 10 km to the southeast, the average area of the landslide again reaches its peak. According to the inversion results of Yang et al. (2022), this may result from the central location of the rupture not coinciding with the initial rupture location (seismic positioning results). The former is 10 km away from the latter in the strike direction. Therefore, according to the distribution and area characteristics of the landslide, it is speculated that the surface fracture is likely to occur near the Moxi fault 0–10 km northwest and 8–18 km southeast of the epicenter.

Since 1700, there have been 9 earthquakes with magnitude above 7 along the entire Xianshuihe fault zone, which occurred once every 36 years on average. Almost the whole fault system north of Moxi fault has undergone seismic surface rupture (Bai et al. 2022) (Fig. 12a). The Ms6.8 Luding earthquake has been 49 years since the last major earthquake (Luhuo earthquake of magnitude M7.6 in 1973). It is the result of the release of stress accumulation along the Xianshuihe fault zone under the background of the convergence of the India Eurasian plate and the continuous southeastward extrusion of the Bayan Har block. Relevant researches show that after the Wenchuan earthquake in 2008 and the Lushan earthquake in 2013, the Coulomb failure stress changes (ΔCFS) near the Xianshuihe fault increased significantly, and the slip rate along the fault increased from northwest to southeast (Xu et al. 2013b; Wu et al. 2014; Xiong et al. 2016). The earthquake released the accumulated strain energy in the Moxi section, but there is still possibility of inducing large earthquakes in the south of the Xianshuihe fault system (such as the Anninghe fault, Daliangshan fault, etc.) in the future.

Innovation and limitation

As of the submission of this manuscript, there is still a lack of research on the secondary disasters triggered by the Luding Ms 6.8 earthquake. The casualties and economic losses caused by the earthquake are huge, so the results obtained in the manuscript will provide an important guideline for future disaster prevention and mitigation in the region. As described in the previous discussion, although the research methods used in this paper are common, the landslide database used in this paper is the most perfect at present, and the research results have also been verified by field work. At the same time, this is also the first applied study of this landslide inventory, which indirectly confirmed the accuracy of the inventory.

The lack of remote sensing data in some regions of the study area is the defect of this study. However, from the field work, this defect did not have an important impact on the research results. In addition, the environmental factors used in this study are obtained according to relevant research and universal recognition, and cannot fully represent the causes and control factors of landslides.

Conclusions

(1) Based on the inventory of coseismic landslides in the Luding earthquake, the distribution characteristics of coseismic landslides is analyzed from three aspects of earthquake, geology, and topography. The results show that the landslide is more likely to develop in the area with slope of more than 40°, slope direction of 67.5–112.5 degree, and vegetation coverage of 40–50%. Granite areas and forest areas are more conducive to landslide development.

The closer to the active fault, the more the coseismic landslides are. The correlation between the two parameters is better than that between the distance from the seismogenic fault and the coseismic landslide development. This shows that the development of coseismic landslide is not only affected by the seismogenic fault but also controlled by other active faults.

(2) There are 5007 coseismic landslides in the Luding earthquake VII-degree area and above, with a total area of 17.36 km^2. The landslides are generally distributed along the NW–SE direction. Most landslides are medium and small rock collapses and destructive debris flows, with a small number of large-scale landslides. The highest landslide area density is 13.8%, and the highest point density of the landslide is 35.73 km^2. High density area is mainly concentrated in the IX-degree area and the northeast side of the seismogenic fault.

Author contributions

C.X. designed the framework of this paper. Z.C. provided the text of introduction. X.H. and X.X. provided the text and pictures related to geological structure in this paper. Y.H. provided the text and pictures of Sect. 3.2. X.S. provided the text and pictures of Sect. 3.1 and Sect. 4.1. C.X. and T.L provided the text and pictures of Sect. 5.2. Z.X. summarized all materials and wrote the article.

Funding

This study was supported by National Institute of Natural Hazards, Ministry of Emergency Management of China (Grant Number: ZDJ2022-20), the National Natural Science Foundation of China (42077259).

Availability of data and materials

The data that support the findings of this study are openly available in "Appendix A. Supplementary data" at https://doi.org/10.1016/j.eqrea.2022.100181

Declarations

Competing interests

The authors declare that they have no conflict of interest.

Received: 5 December 2022 Accepted: 30 January 2023
Published online: 04 February 2023

References

Allen CR, Luo Z et al (1991) Field study of a highly active fault zone: the Xianshuihe fault of southwestern China. Geol Soc Am Bull 103:1178–1199. https://doi.org/10.1130/0016-7606(1991)103%3c1178:FSOAHA%3e2.3.CO;2

Bai M, Chevalier ML et al (2021) Spatial slip rate distribution along the SE Xianshuihe fault, eastern Tibet, and earthquake hazard assessment. Tectonics 40:e2021TC006985. https://doi.org/10.1029/2021TC006985

Bai M, Chevalier ML et al (2022) Late Quaternary slip rate and earthqukae hazard along the Qianning segment, Xianshuihe fault. Acta Geol Sin 96(7):2312–2332. https://doi.org/10.19762/j.cnki.dizhixuebao.202214

Chang M, Cui P et al (2021) The spatial distribution characteristics of coseismic landslides triggered by the Ms7.0 Lushan earthquake and Ms7.0 Jiuzhaigou earthquake in southwest China. Environ Sci Pollut Res 28(16):20549–20569. https://doi.org/10.1007/s11356-020-11826-5

Chen XL, Yu L et al (2013) Brief communication: landslides triggered by the Ms = 7.0 Lushan earthquake, China. Nat Hazard 14:1257–1267. https://doi.org/10.5194/nhess-14-1257-2014

Cui YL, Hu JH et al (2022) Landslides triggered by the 1970 Ms 7.7 Tonghai earthquake in Yunnan, China: an inventory, distribution characteristics, and tectonic significance. J Mt Sci 19(6):1633–1649. https://doi.org/10.1007/s11629-022-7321-x

Dai F, Tu X et al (2011) Rock avalanches triggered by oblique-thrusting during the 12 May 2008 Ms 8.0 Wenchuan earthquake, China. Geomorphology 132:300–318. https://doi.org/10.1016/j.geomorph.2011.05.016

Deng Q, Zhang P et al (2003) Basic characteristics of active tectonics of China. Sci China Ser D Earth Sci 46(4):356–372. https://doi.org/10.1360/03yd9032

Fan X, Wang X et al (2022) Characteristics and spatial distribution pattern of Ms 6.8 Luding earthquake occurred on September 5, 2022. J Eng Geol 30:1504–16 (**In Chinese with English abstract**)

Gorum T, Korup O et al (2014) Why so few? Landslides triggered by the 2002 Denali earthquake, Alaska. Quatern Sci Rev 95:80–94. https://doi.org/10.1016/j.quascirev.2014.04.032

Guo R, Zheng Y et al (2018) Locking status and earthquake potential hazard along the middle-south Xianshuihe fault. Remote Sens 10:2048. https://doi.org/10.3390/rs10122048

Guzzetti F, Mondini AC et al (2012) Landslide inventory maps: new tools for an old problem. Earth Sci Rev 112(1):42–66. https://doi.org/10.1016/j.earscirev.2012.02.001

Harp EL, Keefer DK et al (2011) Landslide inventories: the essential part of seismic landslide hazard analyses. Eng Geol 122(1):9–21. https://doi.org/10.1016/j.enggeo.2010.06.013

He X, Xu C (2022) Spatial distribution and tectonic significance of the landslides triggered by the 2021 Ms 6.4 Yangbi earthquake, Yunnan, China. Front Earth Sci. https://doi.org/10.3389/feart.2022.1030417

He X, Xu C et al (2021) Landslides triggered by the 2020 Qiaojia M_w51 earthquake, Yunnan, China: distribution, influence factors and tectonic significance. J Earth Sci 32(5):1056–1068. https://doi.org/10.1007/s12583-021-1492-1

He Q, Wang M et al (2021) Rapidly assessing earthquake-induced landslide susceptibility on a global scale using random forest. Geomorphology 391:107889. https://doi.org/10.1016/j.geomorph.2021.107889

Huang R, Li W (2009) Fault effect analysis of geo-hazard triggered by Wenchuan earthquake. J Eng Geol 17(1):19–28 (**In Chinese with English abstract**)

Huang Y, Xie C et al (2022a) An open-accessed inventory of landslides triggered by the Ms 6.8 Luding earthquake, China on 5 September 2022. Earthq Res Adv. https://doi.org/10.1016/j.eqrea.2022.100181

Huang Y, Xu C et al (2022b) Bibliometric analysis of landslide research based on the WOS database. Nat Hazards Res 2(2):49–61. https://doi.org/10.1016/j.nhres.2022.02.001

Kato N, Lei X et al (2007) A synthetic seismicity model for the Xianshuihe fault, southwestern China: simulation using a rate-and state-dependent friction law. Geophys J Int 169:286–300. https://doi.org/10.1111/j.1365-246X.2006.03313.x

Keefer DK (2000) Statistical analysis of an earthquake-induced landslide distribution—the 1989 Loma Prieta California event. Eng Geol 58(3–4):231–249. https://doi.org/10.1016/S0013-7952(00)00037-5

Li C, Wang X et al (2019) National 1:200000 digital geological map (public version) spatial database. Geol China 46(S1):1–10 (**In Chinese with English abstract**)

Li W, Chen J et al (2022) Emergency analysis of the impact of the Luding Ms 6.8 earthquake on Hailuogou glacier. Geomat Inf Sci Wuhan Univ. https://doi.org/10.13203/J.whugis20220593. (**In Chinese with English abstract**)

Mahdavifar MR, Solaymani S et al (2006) Landslides triggered by the Avaj, Iran earthquake of June 22, 2002. Eng Geol 86(2–3):166–182. https://doi.org/10.1016/j.enggeo.2006.02.016

Meunier P, Uchida T et al (2013) Landslide patterns reveal the sources of large earthquakes. Earth Planet Sci Lett 363:27–33. https://doi.org/10.1016/j.epsl.2012.12.018

Pan J, Li H et al (2020) A newly discovered active fault on the Selaha-Kangding segment along the SE Xianshuihe fault: the South Mugecuo fault.

Acta Geol Sin 94(11):3178–3188. https://doi.org/10.19762/j.cnki.dizhixuebao.2020196. (**In Chinese with English abstract**)
Planet Team (2022) Planet application program interface: in space for life on earth. San Francisco. https://api.planet.com
Shan B, Xiong X et al (2009) Stress changes on major faults caused by M_w7.9 Wenchuan earthquake, May 12, 2008. Sci China Ser D Earth Sci 52(5):593–601. https://doi.org/10.1007/s11430-009-0060-9
Shao X, Xu C (2022) Earthquake-induced landslides susceptibility assessment: a review of the state-of-the-art. Nat Hazards Res 2(3):172–182. https://doi.org/10.1016/j.nhres.2022.03.002
Shao X, Xu C et al (2022) Two public inventories of landslides induced by the 10 June 2022 Maerkang Earthquake swarm, China and ancient landslides in the affected area. Nat Hazards Res. https://doi.org/10.1016/j.nhres.2022.09.001
Tang R, Qiang H et al (1984) On the seismogeological setting and conditions of seimogenic stuctures of 1981 Daofu earthquake. Seismol Geol 6(2):33–41 (**In Chinese with English abstract**)
Tapponnier P, Molnar P (1977) Active faulting and tectonics in China. J Geophys Res Earth Surf 82(20):2905–2930. https://doi.org/10.1029/JB082i020p02905
Tapponnier PE, Xu Z et al (2001) Oblique stepwise rise and growth of the Tibet Plateau. Science 294:1671–1677. https://doi.org/10.1126/science.105978
Tatard L, Grasso JR (2013) Controls of earthquake faulting style on near field landslide triggering: the role of coseismic slip. J Geophys Res Solid Earth 118(6):2953–2964. https://doi.org/10.1002/jgrb.50215
Tie Y, Zhang X et al (2022) Characteristics of geological hazards and it's mitigations of the *Ms*6.8 earthquake in Luding County. Sichuan Province. Hydrogeol Eng Geol 49(6):1–12 (**In Chinese with English abstract**)
Toda S, Lin J et al (2008) 12 May 2008 M = 7.9 Wenchuan, China, earthquake calculated to increase failure stress and seismicity rate on three major fault systems. Geophys Res Lett 35:L17305. https://doi.org/10.1029/2008GL034903
Valagussa A, Marc O et al (2019) Seismic and geological controls on earthquake-induced landslide size. Earth Planet Sci Lett 506:268–281. https://doi.org/10.1016/j.epsl.2018.11.005
Wang E, Burchfiel BC (2000) Late cenozoic to Holocene deformation in southwestern Sichuan and adjacent Yunnan, China, and its role in formation of the southeastern part of the Tibetan Plateau. Geol Soc Am Bull 112(3):413–423. https://doi.org/10.1130/0016-7606(2000)112
Wang M, Li T et al (2015) Back analysis of stress field in the intersection region of Y shaped fault, Sichuan. J Railw Sci Eng 12(5):1088–1095. https://doi.org/10.19713/j.cnki.43-1423/u.2015.05.016. (**In Chinese with English abstract**)
Wang X, Fang C et al (2022) Research on emergency evaluation of landslides induced by Luding Ms 6.8 earthquake. Geomat Inf Sci Wuhan Univ. https://doi.org/10.13203/j.whugis20220586. (**In Chinese with English abstract**)
Wen X, Allen CR et al (1989) Segmentation, geometric features, and theirseismotectonic implications for the Holocene Xianshuihe fault zone. Acta Seismol Sin 11(4):362–372 (**In Chinese with English abstract**)
Wen X, Ma S et al (2008) Historical pattern and behavior of earthquake ruptures along the eastern boundary of the Sichuan-Yunnan faulted-block, southwestern China. Phys Earth Planet Inter 168:16–36. https://doi.org/10.1016/j.pepi.2008.04.013
Wu P, Li Z et al (2014) Numerical simulation of stress evolution on Xianshuihe fault based on contact element model. Prog Geophys 29(5):2084–2091. https://doi.org/10.6038/pg20140514. (**In Chinese with English abstract**)
Wu C, Cui P et al (2018) Seismogenic fault and topography control on the spatial patterns of landslides triggered by the 2017 Jiuzhaigou earthquake. J Mt Sci 15:793–807. https://doi.org/10.1007/s11629-017-4761-9
Xiong W, Tan K et al (2016) Triggering of Mw5.9 Kangding earthquake bu Coulomb stress evolution along Xianshuihe fault zone since 1995. J Geod Geodyn 36(2):95–100. https://doi.org/10.14075/j.jgg.2016.02.001. (**In Chinese with English abstract**)
Xu C, Xu X (2014) Statistical analysis of landslides caused by the Mw 6.9 Yushu, China, earthquake of April 14, 2010. Nat Hazards 72(2):871–893. https://doi.org/10.1007/s11069-014-1038-2
Xu C, Xu X et al (2013a) Detailed catalog of landslides triggered by the 2008 Wenchuan earthquake and statistical analyses of their spatial distribution. J Eng Geol 21(1):25–44. https://doi.org/10.3969/j.issn.1004-9665.2013.01.004. (**In Chinese with English abstract**)
Xu J, Shao Z et al (2013b) Evolution of Coulomb stress and stress interaction among strong earthquakes along the Xianshuihe fault zone. Chin J Geophys 56(4):1146–1158. https://doi.org/10.6038/cjg20130410. (**In Chinese with English abstract**)
Xu C, Xu X et al (2014) Three (nearly) complete inventories of landslides triggered by the May 12, 2008 Wenchuan Mw 7.9 earthquake of China and their spatial distribution statistical analysis. Landslides 11(3):441–461. https://doi.org/10.1007/s10346-013-0404-6
Yang X, Yao Y (2018) Development and distribution characteristics of geological hazards after the 2014 Ludian M_S6.5 earthquake. China Earthq Eng J 40(5):1078–1083. https://doi.org/10.3969/j.issn.1000-0844.2018.05.1078. (**In Chinese with English abstract**)
Yang Z, Dai D et al (2022) Rupture process and aftershock mechanisms of the 2022 Luding Ms 6.8 earthquake in Sichuan, China. Earthq Sci 35:1–2. https://doi.org/10.1016/j.eqs.2022.09.001
Yin Y (2009) Features of landslides triggered by the Wenchuan earthquake. J Eng Geol 17(1):29–38 (**In Chinese with English abstract**)
Zhang P (2013) A review on active tectonics and deep crustal processes of the Western Sichuan region, eastern margin of the Tibetan Plateau. Tectonophysics 584:7–22. https://doi.org/10.1016/j.tecto.2012.02.021
Zhang X, Lei L et al (2022) Large-scale landslide inventory and their mobility in Lvliang City, Shanxi Province. China Nat Hazards Res 2(2):111–120. https://doi.org/10.1016/j.nhres.2022.05.002
Zhao B, Wang Y et al (2021) The Mogangling giant landslide triggered by the 1786 Moxi M 7.75 earthquake. China Nat Hazards 106:459–485. https://doi.org/10.1007/s11069-020-04471-1
Zheng G, Wang H et al (2017) Crustal deformation in the India-Eurasia collision zone from 25 years of GPS measurements. J Geophys Res Solid Earth 122:9290–9312. https://doi.org/10.1002/2017JB014465

Publisher's Note